RSC Advances

This is an *Accepted Manuscript*, which has been through the Royal Society of Chemistry peer review process and has been accepted for publication.

Accepted Manuscripts are published online shortly after acceptance, before technical editing, formatting and proof reading. Using this free service, authors can make their results available to the community, in citable form, before we publish the edited article. This *Accepted Manuscript* will be replaced by the edited, formatted and paginated article as soon as this is available.

You can find more information about *Accepted Manuscripts* in the **Information for Authors**.

Journal Name

ARTICLE

One-pot Synthesis of Novel Hierarchical Bifunctional Ga/HZSM-5 Nanosheets for Propane Aromatization

Wannaruedee Wannapakdee[a], Chularat Wattanakit*[a], Veerachart Paluka[b], Thittaya Yutthalekha[a], Jumras Limtrakul[c]

Hierarchical galloaluminosilicate nanosheets with the MFI structure have been successfully prepared by a one-pot hydrothermal process. The tetrabutylphosphonium hydroxide (TBPOH), a dual structure-directing agent (SDA), was used to simultaneously produce the MFI structure and the self-assemblies of nanolayers. The as-synthesized samples were characterized by means of XRD, TEM, SEM, EDS, ICP, ^{27}Al MAS NMR, FTIR, H_2-TPR, NH_3-TPD and N_2 physisorption. The galloaluminosilicate nanosheets exhibit the outstanding properties, such as an extremely high meso/macroporosity (to be five to six orders of magnitude higher compared with the conventional zeolite), a uniform Si, Al and Ga distribution, along with the appropriate acidic properties. The galloaluminosilicate nanosheets can greatly enhance the catalytic performances in terms of activity (60 and 20% for propane conversion over the hierarchical Ga/HZSM-5 and the conventional zeolite, respectively), BTX selectivity (almost three times higher compared with the conventional zeolite), and significant reduction of deposited coke (approximately by 70%) for converting of propane at 823 K under an atmospheric pressure without any special pre-treatments of catalysts. This first example demonstrates the simple and low-cost approach for the synthesis of hierarchical bifunctional zeolite nanosheets and the challenging for the development of heterogeneous catalysts.

Introduction

Zeolites are regularly the crystalline aluminosilicates with a well-defined three-dimensional structure. Their crystalline framework directly provides the outstanding properties, such as high thermal/chemical stabilities, tunable acid-basic properties and shape selectivities. As a result, they have played an important role in various potential applications ranging from adsorption to separation and catalysis.[1-5] Due to the microporous feature of zeolites, they often suffer from disadvantages, such as low external surface areas, low accessible active sites, mass/heat transfer limitation and short catalyst lifetime.[6] To overcome these drawbacks, there are several approaches to be demonstrated, for example, making zeolites having nanocrystal sizes, resulting in shortening the diffusion path length.[7-9] Although the zeolite nanocrystals exhibit great external surface areas and provide the

fast diffusion of guest molecules to accessible active sites,[10, 11] the zeolite nanocrystals also suffer from an increase of pressure drop in a packed-bed reactor and a high cost of the synthesized process due to their difficult separation after synthesis or/and reaction processes.[6] An alternative way to improve the efficiency of conventional zeolites is to design the zeolites with hierarchical porous structures, namely hierarchical zeolites. These materials compose of at least two levels of porosity such as micro-mesoporous or micro-macroporous or micro-meso-macroporous structures. Recently, the hierarchical zeolite nanosheets have been successfully prepared by various approaches.[12-14] The advantages of these materials are not only to greatly decrease diffusion limitation due to reducing their diffusion path length, but also to generate a secondary porous structure between their layers. This results in the addition of the meso/macroporous molecular highway connected to the microporous diffusion path providing high accessible active sites.

In 2009, Choi et al.[15] have discovered a new synthetic route by using the designed diquaternary ammonium-type surfactant ($C_{22}H_{45}$-$N_1(CH_3)_2$-C_6H_{12}-$N_1(CH_3)_2$-C_6H_{13}) as a structure directing agent (SDA) to directly design single-unit-cell MFI nanosheets. The diammonium groups control the microporous MFI structure, while a long hydrophobic chain forming a micelle structure, resulting in preventing the zeolite growth along the b-axis to generate 2D zeolite nanolayers. Recently, Wueyi Zhang et al.[16] demonstrated the synthesis of self-pillared MFI nanosheets by repetitive branching. The tetrabutylphosphonium hydroxide (TBPOH) was also used as a bifunctional structure agent controlling the structures of microporous MFI and 2D nanolayers, resulting in the formation of a

a. Department of Chemical and Biomolecular Engineering, School of Energy Science and Engineering, Vidyasirimedhi Institute of Science and Technology, Rayong 21210 Thailand.
Email: chularat.w@vistec.ac.th; fax +66 3301 4445 ext 2176
b. Department of Chemistry and NANOTEC Center for Nanoscale Materials Design for Green Nanotechnology, Kasetsart University, Bangkok 10900, Thailand.
c. Department of Materials Science and Engineering, School of Molecular Science and Engineering, Vidyasirimedhi Institute of Science and Technology, Rayong 21210 Thailand.
† Electronic Supplementary Information (ESI) available: Particle size distribution (S1), Distribution of nanolayer thickness (S2), A) N_2 adsorption/desorption isotherms and B) BJH pore size distribution (S3), ^{27}Al MAS NMR spectra (S4), and TGA curves (S5).]. See DOI: 10.1039/x0xx00000x

house of cards structure by repetitive branching of MFI nanosheets. Although there are several synthetic approaches to be revealed for the preparation of hierarchical MFI nanosheets, there are only a few works focusing on the direct synthesis of ZSM-5 nanosheets by using a phosphonium structure-directing agent (SDA). This type of template also has many advantages, such as its low cost and high stability compared with other quaternary ammonium surfactants.[17]

In addition to the aluminosilicate zeolites, the incorporation of metal atoms to the zeolite framework exhibits the interesting properties.[18] In particular, the gallium-incorporated zeolites are the effective bifunctional catalysts for converting light alkanes to aromatics.[19] These materials are not only to improve the aromatic yield but also to increase the catalyst stability due to a relative decrease of acid strength compared with the aluminosilicate zeolites. This behavior leads to a significant decrease of coke formation.[20-22]

The conversion of propane to high value-added aromatic products, such as benzene, toluene and xylene (BTX), is an interesting issue in both academic and petrochemical industrial points of view.[23] Several studies have shown that the bifunctional gallium loaded HZSM-5 is one of the most suitable catalysts for aromatization of propane.[23-25] The Ga species have played an important role for the dehydrogenation of propane to propylene, while the Brønsted acid sites of zeolite promote the oligomerization of olefins and the subsequent aromatization to produce the aromatics.[26-29] Typically, the Ga/ZSM-5 has been prepared by the post synthesis treatment, such as an impregnation, and an ion-exchange. The gallium species obtained by these two methods are not active without a special treatment. In addition, the gallium species are aggregated on external surfaces of zeolites, resulting in losing of the catalytic activity.[28,30] In contrast, the Ga/HZSM-5 obtained from an *in-situ* hydrothermal method gives a higher aromatic yield for the aromatization of light alkanes due to highly dispersed active gallium species in close vicinity to Brønsted acid sites.[31-33] However, it often suffers from the fast deactivation of catalysts. This might be the relatively large amount of deposited coke on surfaces.[25,34-36]

To improve the efficiency of catalysts for converting propane to aromatics, Yassir *et al.*[37] reported the benefits of mesoporous galloaluminosilicates for the aromatization of propane. Hierarchical Ga/HZSM-5 was prepared by three-step modifications, involving the direct-hydrothermal synthesis of conventional Ga/HZSM-5, the steaming of the obtained zeolites and the subsequent hydrolysis of steam–treated zeolites in the presence of surfactant to generate the mesoporous feature. Recently, Ogunronbi *et al.*[38] reported the synthesis of the hierarchical Ga-containing HZSM-5 zeolite by a top-down post-synthesis method (e.g., desilication, alkaline treatment, CTAB-mediated assembly of Ga-containing zeolite seed into MCM-41 mesostructure, *etc.*). Although there are some reports describing the synthesis of mesoporous galloaluminosilicates, most of them have focused on the post synthesis treatment, which requires several steps of preparation. To date, the design of the galloaluminosilicate with hierarchical nanosheet structure has not yet been demonstrated.

In the present study, we report the synthesis of hierarchical galloaluminosilicate nanosheets with the MFI framework by a one-pot hydrothermal method. The tetra(*n*-butyl)phosphonium hydroxide (TBPOH) was used as a dual functional template to simultaneously control both the MFI

structure and hierarchical nanosheet assemblies. This first example of the hierarchical Ga/HZSM-5 nanosheets, obtained by a one-step synthesis method without any special treatments, exhibits an excellent catalytic application for converting propane to aromatics (BTX) in terms of activity, selectivity and catalyst lifetime.

Experimental

Catalyst Preparation

MFI-type galloaluminosilicate nanosheets were hydrothermally synthesized by using a tetra(*n*-butyl)phosphonium hydroxide (TBPOH) as the SDA. The molar composition of the synthesis gel was $60SiO_2/$ $0.40Al_2O_3/$ $0.60Ga_2O_3/$ $18TBPOH/$ $0.75NaOH/$ $240EtOH/$ $600H_2O$. In a typical procedure, the first solution containing 0.0530 g of aluminum isopropoxide (Sigma-Aldrich, ≥ 98.0%), 0.0343 g of gallium nitrate (Sigma-Aldrich, 99.9%) and 8.6780 g of tetraethyl orthosilicate (Sigma-Aldrich, ≥ 99.0%) was prepared. The second solution containing 8.6250g of TBPOH solution (Sigma-Aldrich, 40% in H_2O) and 0.200 g of sodium hydroxide (Sigma-Aldrich, ≥98.0%) in 2.3250 g of distilled water was added into the first solution under vigorous stirring. The resultant gel was continuously stirred at room temperature for 12 h to obtain a homogenous mixture. The obtained gel was transferred to a Teflon lined stainless steel autoclave and heated at 403 K for 48 h. The precipitated product was collected and washed with distilled water by repeated centrifugation until the pH of filtrate less than 9. The product was dried overnight at 373 K, and then finally calcined in air at 923 K for 8 h to remove the SDA. The synthesized product was converted to the H$^+$ form by an ion-exchange with 1 M NH_4NO_3 solution at 353 K for three times. The obtained solid was dried and finally calcined in air at 923 K for 6 h. The obtained MFI-type galloaluminosilicate nanosheet is denoted as the Ga-HZSM-5-NS. The MFI-type aluminosilicate nanosheet (HZSM-5-NS) was synthesized without the addition of gallium precursor by following the literature procedures.[16] The conventional MFI-type galloaluminosilicate (Ga-HZSM-5-CON) was synthesized by using TPAOH as the SDA and the gel precursor was crystallized at 453 K for 3 d. The molar composition of a synthesis gel is $10SiO_2/$ $0.05Al_2O_3/$ $0.10Ga_2O_3/$ $1TPAOH/$ $1.03NaOH/$ $240EtOH/$ $400H_2O$. The obtained product was filtered, washed with DI water and dried at 373 K overnight. Finally, the product was calcined at 923 K for 8 h to remove the SDA. The conventional MFI-type aluminosilicate (HZSM-5-CON) was obtained by the similar procedure in the absence of the gallium precursor.

Catalyst Characterization

Powder X-ray diffraction (XRD) patterns of the as-synthesized samples were investigated by using a Bruker D8 ADVANCE diffractometer and CuKα radiation (30 kV, 40 mA) with step size of 0.02 and scan rate of 1° min^{-1}. The relative crystallinity of synthesized samples was estimated based on the intensity of the peaks of 2θ = 22-25. Scanning electron microscopy (SEM) images and transmission electron microscopy (TEM) images were recorded by the JEOL JSM-7600F (at 2 kV) and JEOL JEM-2010 microscope operated at 200 kV, respectively. The composition and elemental distribution of synthesized samples were measured by an inductively coupled plasma analysis, ICP-OES, using a model Agilent technologies 715 and an energy dispersive spectroscopy, EDS,

respectively. ^{27}Al MAS NMR spectroscopy performed on an AVANCE 300 MHZ Digital NMR spectrometer (Bruker Biospin; DPX-300) was used to investigate the nature of aluminium species. The textural properties were determined by a N_2 adsorption/desorption technique at 77 K performed on a Micromeritics ASAP 2020 apparatus. The specific surface area (S_{BET}), micropore surface area and pore volume, mesopore size distribution were calculated by the Brunauer-Emmett-Teller (BET) method, t-plot method and Barrett-Joyner-Halenda (BJH) model, respectively.[39]

The H_2 temperature programmed reduction (H_2-TPR) and NH_3 temperature programmed desorption (NH_3-TPD) measurements were carried out in a fixed-bed reactor system equipped with a TCD detector. Typically, the samples (0.3 g) were pre-treated at 823 K for 2 h with heating rate of 10 K/min under the flow of N_2 and then cooled down to a desired temperature. In the case of the H_2-TPR experiments, the temperature was increased from 323 to 1173 K with the heating rate of 5 K/min in a flow of 2v/v% of H_2 in Ar (5 ml/min). In the NH_3-TPD experiment, the sample was equilibrated with 5% of NH_3 in He for 30 min at 323 K and then purged with He for 1 h to remove the weak adsorbed NH_3. The NH_3 TPD profiles were recorded by increasing the temperature from 323 K to 1073 K with the heating rate of 5 K/min in the flow of He (30 ml/min).

Propane Aromatization

The conversion of propane to aromatics was carried out in a continuous-flow fixed-bed reactor. A 0.3 g of catalyst was placed into the reactor. Prior to the catalytic studies, zeolite samples were activated at 823 K in the flow of N_2 (2.5 ml/min) for 2 h. The feed was the propane in N_2 with the molar volume ratio of 1:1. All reactions were carried out at 823 K, GHSV (gas hourly space velocity) of 300 h^{-1}, and atmospheric pressure. The analysis of the reaction mixtures was performed by an on-line gas chromatograph (GC) (Agilent 7820A) equipped with a FID detector and a GS-GASPRO capillary column (60 m x 0.320 mm) at an interval time of 1 h. The mass balance was checked for all experiments (98.65 ± 1.32%). The conversion of feed (X_{feed}) and product selectivity (S_i) are reported in the mole percentage and calculated by the following equations:

$$X_{feed}(\%) = (\frac{\sum A_i - A_{unreacted\_feed}}{\sum A_i}) \times 100\%$$

$$S_i(\%) = (\frac{A_i}{\sum A_i - A_{unreacted\_feed}}) \times 100\%$$

Where $\sum A_i$ and $A_{unreacted\_feed}$ are the corrected chromatographic areas of species i and remaining propane, respectively.

Results and Discussions

Fig. 1 shows the XRD patterns of all as-synthesized samples. The characteristic diffraction patterns of HZSM-5-NS and HZSM-5-CON were identical to the typical reflection characteristic of the MFI framework structure, confirming that the synthesized aluminosilicates compose of a highly crystalline MFI framework without the contamination of any other crystalline phases. Ga-containing samples (Ga-HZSM-5-NS and Ga-HZSM-5-CON) also were the highly crystalline MFI.

The relative crystallinity of Ga-containing samples was slightly higher compared with that of the corresponding HZSM-5 samples. In addition, no XRD characteristic peaks assigned to be the bulk β-Ga_2O_3 was observed in the MFI-type galloaluminosilicates, implying that the Ga species appear as highly-dispersed species in the form of either gallium oxide species with small size (< 4 nm) or the Ga framework.[40]
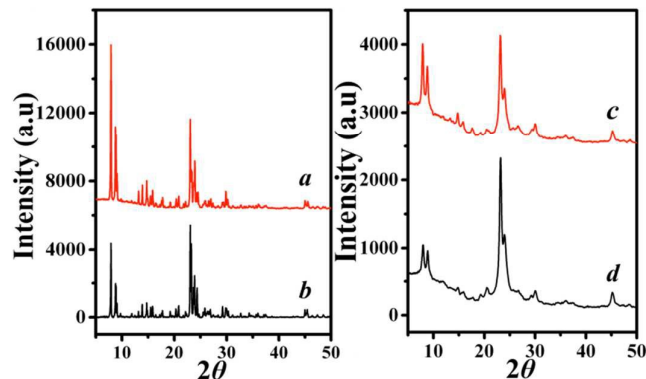

Fig. 1. XRD patterns of (a) HZSM-5-CON, (b) Ga-HZSM-5-CON (c) HZSM-5-NS, and (d) Ga-HZSM-5-NS.

The scanning electron micrographs reveal the morphologies of as-synthesized samples (Fig. 2). According to the conventional zeolite samples, cubic-shaped crystals with particle sizes of 368±36 and 412±32.5 nm were observed for the HZSM-5-CON and the Ga-HZSM-5-CON, respectively (see the particle size distribution in Fig. S1(a-b) in Supporting Information). In strong contrast to this, the spherical assemblies of ZSM-5 nanolayers were observed in the case of the HZSM-5-NS and the Ga-HZSM-5-NS. The particle size distribution of their assemblies and the nanosheet thickness are shown in Fig. S1(c-d) and Fig. S2(a-b) in the Supporting Information, respectively. The particle size and the nanosheet thickness of the galloaluminosilicate nanosheets insignificantly change compared with the aluminosilicate nanosheets. This indicates that the gallium incorporation into the zeolite framework does not change the morphologies of zeolites.

Fig. 2. SEM images of (a) HZSM-5-CON, (b) Ga-HZSM-5-CON (c)
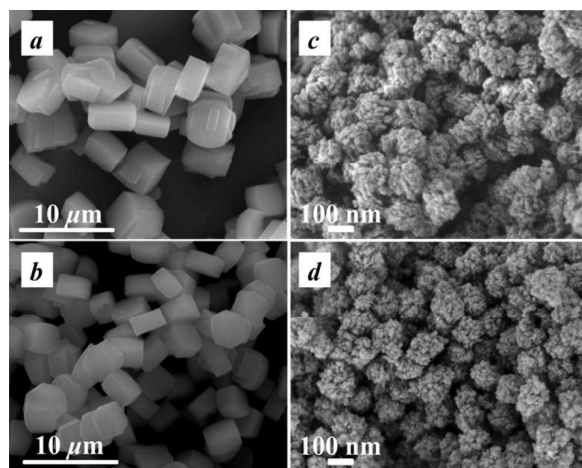
HZSM-5-NS and (d) Ga-HZSM-5-NS.

The TEM images of the Ga-HZSM-5-NS also confirm their highly uniform particle size distributions (Fig. 3(a) for TEM images of the Ga-HZSM-5-NS). The HRTEM reveals that the Ga-HZSM-5-NS composes of the house of cards structure of zeolite nanolayers with the nanosheet thickness of 9.81 nm and the lattice fringes also confirm the presence of the polycrystalline structure in the assemblies of nanolayers (Fig. 3(b) and Fig. S2(a-b) in Supporting Information).
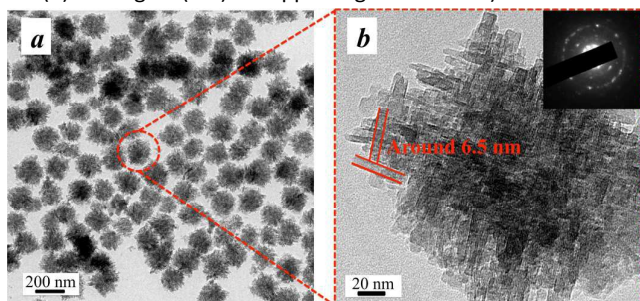

Fig. 3. (a) TEM images of the Ga-HZSM-5-NS and (b) High-resolution TEM images of the Ga-HZSM-5-NS. The inset in (b) is the selected-area-diffraction (SAD) pattern of the high-resolution image.

The elemental composition of Si, Al and Ga and their distributions of the Ga-HZSM-5-NS were obtained by ICP-OES and EDS mapping as shown in Table 1 and Fig. 4. The SiO_2/Al_2O_3 and Ga/(Al+Ga) ratios obtained by ICP-OES of all as-synthesized samples are approximately by 63 and 0.72, respectively, which are similar to the values obtained by the EDS analysis (72 and 0.77 for SiO_2/Al_2O_3 and Ga/(Al+Ga), respectively). In addition, the EDS elemental mapping of Si, Al and Ga elements shows the highly uniform distribution of all elements over the entire particle areas.
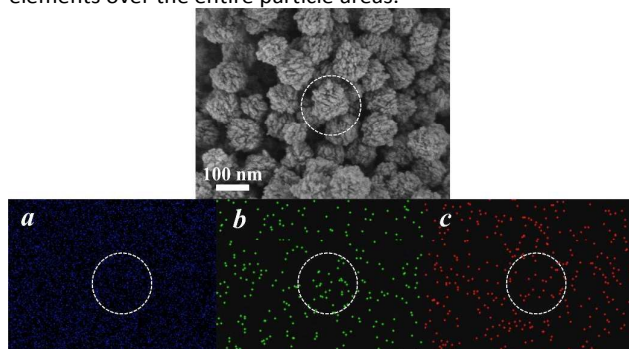

Fig. 4. EDS elemental mapping of the Ga-HZSM-5-NS for (a) Si, (b) Al and (c) Ga elements.

The textural properties of the synthesized samples were investigated by the N_2 physisorption technique as shown in Table 1. The N_2 sorption isotherms of the HZSM-5-CON and the Ga-HZSM-5-CON correspond to a type I isotherm because of the micropore filling[41] (Fig. S3A (a-b) in the Supporting Information). In contrast, the HZSM-5-NS and the Ga-HZSM-5-NS exhibit the combination of the type I isotherm at low relative P/P_0 and the hysteresis loop at high P/P_0 due to a capillary condensation within mesopores and macropores (Fig.S3A (c-d) in the Supporting Information). The pore size distribution (PSD) data derived from the BJH adsorption branch of isotherm reveal a broad distribution of mesopores in the range between 5 and 15 nm (Fig.S3B in the Supporting Information). This behaviour indicates that both aluminosilicate and galloaluminosilicate nanosheets compose of the micropororous feature due to zeolite characteristics and mesopores/macropores obtained from the assemblies of nanolayers and the interparticle voids. This makes it clear that external surface areas and meso/macropore volumes of the HZSM-5- NS and Ga-HZSM-5-NS can be five to six orders of magnitude higher compared with the conventional zeolites. This demonstrates that the designed hierarchical zeolites increase the meso/macroporosity, while the microporosity is significantly preserved.

The nature of aluminium active sites was investigated by ^{27}Al MAS NMR spectroscopy as shown in Fig. S4 in the Supporting Information. A strong peak at the chemical shift about 52.3 ppm, assigned to the tetrahedral coordinated aluminium in frameworks, was observed, whereas no characteristic peak of the octahedrally coordinated extra-framework aluminum species appeared at the chemical shift of 0 ppm. It clearly confirms that the aluminium atoms are most likely to occupy as the Al-substituted zeolite framework, whereas the presence of the extra-framework aluminum species can be omitted even in the galloaluminosilicate samples. This shows that the dealumination was not observed by the Ga incorporation to the zeolite framework during the crystallization.

Fig. 5 shows H_2 TPR curves and NH_3 TPD profiles. According to the H_2 TPR profiles, the three major peaks are observed for the Ga-HZSM-5-NS nanosheets. The first and second peaks at c.a. 833-843 K and c.a. 923-933 K correspond to the reduction of well-dispersed Ga_2O_3 or GaO^+ extraframework. The reduction peak at high temperature (c.a. 1023-1033 °C) can be attributed to the segregated bulk Ga_2O_3 particles.[32] In contrast, the Ga-HZSM-5-CON exhibits the characteristic peaks at higher temperature, indicating that the Ga species in the conventional MFI-type galloaluminosilicate agglomerate into larger Ga_2O_3 particles or preferably situated on the outermost surfaces of the zeolite. The acidity of synthesized nanosheets was investigated by the NH_3 TPD. There are three major desorption peaks at 513, 588, and 648 K assigned to weak, medium and strong acid sites, respectively. With the incorporation of Ga in the zeolite framework, the desorption-peak is shifted to lower temperature, indicating lower acid strength of the Ga-HZSM-5-NS compared with the HZSM-5-NS. In addition, the amount of strong acid sites of the galloaluminosilicate decreases approximately by 6% compared with that of the HZSM-5.

To illustrate the benefits of the Ga-HZSM-5-NS, the conversion of propane to aromatics was studied as the model reaction. Fig. 6A demonstrates the conversion of propane as a function of time-on-stream (TOS). The low activity of propane conversion was observed for the HZSM-5-CON. As expected, the hierarchical MFI nanosheets can significantly enhance the propane conversion. Compared with the HZSM-5-CON, the catalytic activity of the HZSM-5-NS is higher approximately by 1.5 times. Interestingly, the Ga-HZSM-5-NS exhibits the excellent catalytic activity, which can be three orders of magnitude higher compared with another samples. Not only the improved catalytic activity, but also the enhanced selectivity of aromatics (BTX) was observed for the MFI-type galloaluminosilicate nanosheets.

RSC Advances

Table 1. Textural properties of all synthesized samples obtained by N_2 physisorption

Sample	Si/Al[a]	Ga/(Al+Ga)[a]	S_{BET}[b]	S_{micro}[c]	S_{ext}[d]	V_{total}[e]	V_{micro}[f]	V_{ext}[g]	S_{ext}/S_{BET}[h]
HZSM-5-CON	63	0.00	391	307	84	0.17	0.12	0.05	0.21
Ga-HZSM-5-CON	63	0.75	364	328	36	0.14	0.13	0.01	0.10
HZSM-5-NS	60	0.00	542	296	246	0.86	0.12	0.74	0.45
Ga-HZSM-5-NS	65	0.70	531	311	220	0.77	0.10	0.67	0.41

[a]Si/Al and [a]Ga/(Al+Ga) determined by ICP-OES, [b]S_{BET}: BET specific surface area, [c]S_{micro}: micropore surface area, [d]S_{ext}: external surface area, [e]V_{total}: total pore volume obtained at P/P0=0.95, [f]V_{micro}: micropore volume, [g]$V_{ext} = V_{total} - V_{micro}$, [h]Fraction of external surface area.
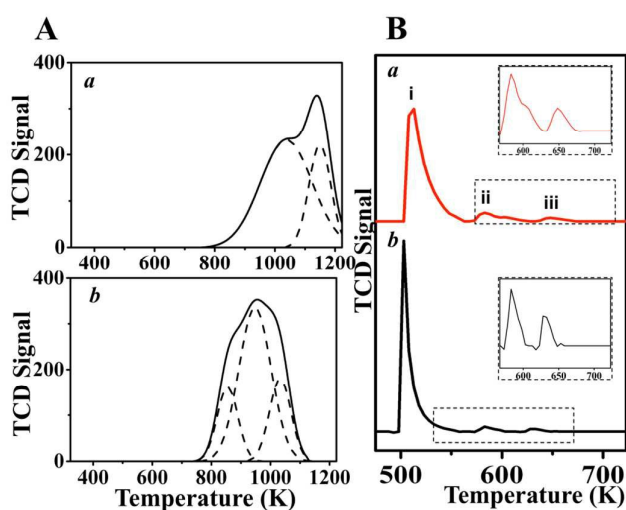

Fig. 5. A) H_2 TPR of (a) Ga-HZSM-5-CON and (b) Ga-HZSM-5-NS and B) NH_3 TPD profiles of (a) HZSM-5-NS and (b) Ga-HZSM-5-NS.

Fig. 6B shows the product selectivity at 24 h of TOS. It clearly shows that the aluminosilicate samples (HZSM-5-CON and HZSM-5-NS) promote the catalytic cracking reaction of propane to produce C1 and C2 as the main products, whereas the aromatic yield is very low. However, the dehydro-cyclization of propane is significantly enhanced by the incorporation of Ga in the MFI structure, resulting in an increase of aromatics and propylene.

This makes it clear that gallium species play an important role in the dehydrogenation of propane to yield the propylene, which is the important intermediate for the further oligomerization and the subsequent cyclization. This could eventually lead to an increased selectivity of the propylene and aromatics (almost 75%) over the Ga-HZSM-5-NS.
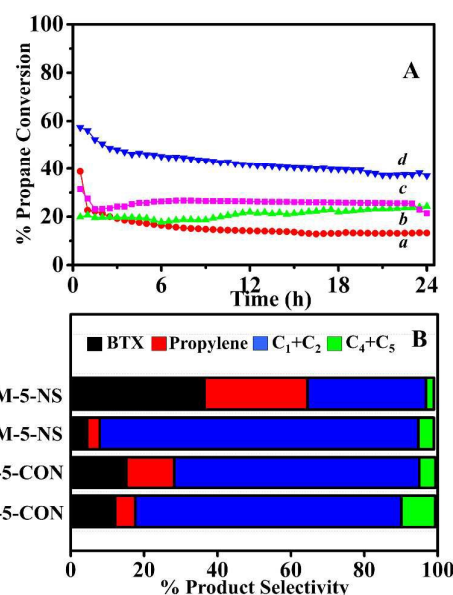

Fig. 6. A) Conversion of propane as a function of time-on-stream (TOS) and B) Product selectivity at 24 h of TOS on (a) HZSM-5-CON, (b) Ga-HZSM-5-CON (c) HZSM-5-NS and (d) Ga-HZSM-5-NS.

To further explain the effect of the hierarchical structure on propane conversion, the amount of deposited coke was also measured by the thermogravimetric analysis (TGA) as shown in Fig. S5. The TGA curves of all catalysts exhibit two main-weight-loss peaks. The peak at 373 K is due to H_2O removal, whereas the peak at 723 K is due to the carbon decomposition. The carbon weight loss over the HZSM-5-CON, the Ga-HZSM-5-CON, the HZSM-5-NS and the Ga-HZSM-5-NS is 18.53, 17.61, 17.16 and 5.35%, respectively. This result suggests that the Ga-HZSM-5-NS not only enhances the catalytic performances in terms of activity and BTX/propylene selectivity, but also reduces the amount of deposited coke, which probably causes the catalyst deactivation. This first example demonstrates that the MFI-type galloaluminosilicate nanosheets can greatly improve the catalytic

performances of propane conversion without any special pre-treatments. This opens up interesting perspectives for the development of bifunctional catalysts with hierarchical structure obtained by a one-pot hydrothermal synthesis for the potential applications, especially in the petrochemical reactions.

Conclusions

Hierarchical MFI-type galloaluminosilicate nanosheets have been successfully prepared by a one-pot hydrothermal synthesis. The TBPOH was used as a dual structure-directing agent (SDA) to simultaneously control the MFI structure and the self-assemblies of nanolayers. They also exhibit the outstanding properties, such as a high meso/macroporosity with the significant amount of microporosity, a uniform Si, Al and Ga distribution, along with an interesting acidic properties compared with the corresponding aluminosilicate. Interestingly, they also show the excellent catalytic performances in terms of activity, BTX and propylene selectivity as well as a significant reduction of deposited coke, for converting of propane without any special pretreatments. This can be attributed to the synergistic effect of the suitable acidity due to the Ga incorporation and the hierarchical structure due to the added meso/macroporous molecular highway, which improves the accessibility of guest molecules into active sites. This first example demonstrates the design of novel hierarchical galloaluminosilicates by a simple and low-cost approach and it also opens up interesting perspectives for the applications of heterogeneous catalysis in petrochemical processes.

Acknowledgements

Reference

1. D. W. Breck, *Zeolite molecular sieves: structure, chemistry, and use*, Wiley, 1973.
2. R. M. Barrer, *Hydrothermal Chemistry of Zeolites.*, 1982.
3. A. Corma, *Chem. Rev.* 1997, **97**, 2373-2419.
4. P. A. Jacobs, E. M. Flanigen, J. C. Jansen and H. van Bekkum, *Introduction to Zeolite Science and Practice*, Elsevier Science, 2001.
5. R. Xu, W. Pang, J. Yu, Q. Huo and J. Chen, *Chemistry of Zeolites and Related Porous Materials: Synthesis and Structure*, Wiley, 2009.
6. L.-H. Chen, X.-Y. Li, J. C. Rooke, Y.-H. Zhang, X.-Y. Yang, Y. Tang, F.-S. Xiao and B.-L. Su, *J. Mater. Chem.* 2012, **22**, 17381-17403.
7. M. E. Davis, C. Saldarriaga, C. Montes, J. Garces and C. Crowdert, *Nature*, 1988, **331**, 698-699.
8. C. C. Freyhardt, M. Tsapatsis, R. F. Lobo, K. J. Balkus Jr and M. E. Davis, *Nature*, 1996, **381**, 295-298.
9. J. Jiang, J. Yu and A. Corma, *Angew. Chem. Int. Ed.* 2010, **49**, 3120-3145.
10. B. J. Schoeman, J. Sterte and J. E. Otterstedt, *Zeolites*, 1994, **14**, 110-116.
11. L. Tosheva and V. P. Valtchev, *Chem. Mater.*, 2005, **17**, 2494-2513.
12. M. Hartmann, *Angew. Chem. Int. Ed.* 2004, **43**, 5880-5882.
13. J. Pérez-Ramírez, C. H. Christensen, K. Egeblad, C. H. Christensen and J. C. Groen, *Chem. Soc. Rev.* 2008, **37**, 2530-2542.
14. S. Lopez-Orozco, A. Inayat, A. Schwab, T. Selvam and W. Schwieger, *Adv. Mater.* 2011, **23**, 2602-2615.
15. M. Choi, K. Na, J. Kim, Y. Sakamoto, O. Terasaki and R. Ryoo, *Nature*, 2009, **461**, 246-249.
16. X. Zhang, D. Liu, D. Xu, S. Asahina, K. A. Cychosz, K. V. Agrawal, Y. Al Wahedi, A. Bhan, S. Al Hashimi, O. Terasaki, M. Thommes and M. Tsapatsis, *Science*, 2012, **336**, 1684-1687.
17. D. Xu, G. R. Swindlehurst, H. Wu, D. H. Olson, X. Zhang and M. Tsapatsis, *Adv. Funct. Mater.* 2014, **24**, 201-208.
18. M. Moliner, *Dalton Trans.* 2014, **43**, 4197-4208.
19. R. Fricke, H. Kosslick, G. Lischke and M. Richter, *Chem. Rev.* 2000, **100**, 2303-2406.
20. G. P. Handreck and T. D. Smith, *J. Catal.* 1990, **123**, 513-522.
21. R. Fricke, H. Kosslick, G. Lischke and M. Richter, *Chem. Rev.* 2000, **100**, 2303-2405.
22. U. V. Mentzel, K. T. Højholt, M. S. Holm, R. Fehrmann and P. Beato, *App. Cat. A: Gen.* 2012, **417–418**, 290-297.
23. C. R. Bayense, A. J. H. P. van der Pol and J. H. C. van Hooff, *App. Cat.* 1991, **72**, 81-98.
24. V. R. Choudhary, A. K. Kinage and T. V. Choudhary, *App. Cat. A: Gen.* 1997, **162**, 239-248.
25. V. R. Choudhary and P. Devadas, *App. Cat. A: Gen.* 1998, **168**, 187-200.
26. C. R. Bayense, A. P. M. Kentgens, J. W. De Haan, L. J. M. Van de Ven and J. H. C. Van Hooff, *J. Phys. Chem.* 1992, **96**, 775-782.
27. D. J. Parrillo, C. Lee, R. J. Gorte, D. White and W. E. Farneth, *J. Phys. Chem.* 1995, **99**, 8745-8749.
28. N. Rane, A. R. Overweg, V. B. Kazansky, R. A. van Santen and E. J. M. Hensen, *J. Catal.* 2006, **239**, 478-485.
29. G. Krishnamurthy, A. Bhan and W. N. Delgass, *J. Catal.* 2010, **271**, 370-385.
30. I. Nowak, J. Quartararo, E. G. Derouane and J. C. Védrine, *App. Cat. A: Gen.* 2003, **251**, 107-120.
31. V. R. Choudhary, A. K. Kinage, C. Sivadinarayana and M. Guisnet, *J. Catal.* 1996, **158**, 23-33.
32. H. Xiao, J. Zhang, X. Wang, Q. Zhang, H. Xie, Y. Han and Y. Tan, *Catal. Sci. Technol.* 2015, **5**, 4081-4090.
33. K. E. Ogunronbi, N. Al-Yassir and S. Al-Khattaf, *J. Mol. Cat. A: Chem.* 2015, **406**, 1-18.
34. V. R. Choudhary, A. K. Kinage, C. Sivadinarayana, P. Devadas, S. D. Sansare and M. Guisnet, *J. Catal.* 1996, **158**, 34-50.
35. T. V. Choudhary, A. Kinage, S. Banerjee and V. R. Choudhary, *Energy and Fuels*, 2006, **20**, 919-922.
36. N. Al-Yassir, M. N. Akhtar and S. Al-Khattaf, *J. Porous Mater.* 2012, **19**, 943-960.
37. N. Al-Yassir, M. N. Akhtar, K. Ogunronbi and S. Al-Khattaf, *J. Mol. Catal. A: Chem.* 2012, **360**, 1-15.
38. K. E. Ogunronbi, N. Al-Yassir and S. Al-Khattaf, *J. Mol. Catal. A: Chem.* 2015, **406**, 1-18.
39. B. C. Lippens and J. H. de Boer, *J. Catal.* 1965, **4**, 319-323.
40. B. Zheng, W. Hua, Y. Yue and Z. Gao, *J. Catal.* 2005, **232**, 143-151.

ARTICLE

41. K. S. W. Sing, D. H. Everett, R. A. W. Haul, L. Moscou, R. A. Pierotti, J. Rouquerol and T. Siemieniewska, *Pure Appl. Chem.* 1985, **57**, 603-619.

39x19mm (300 x 300 DPI)